Salivary gland progenitor cells and epithelium in primary Sjögren's syndrome

Wang, Xiaoyan

DOI:
10.33612/diss.135858262

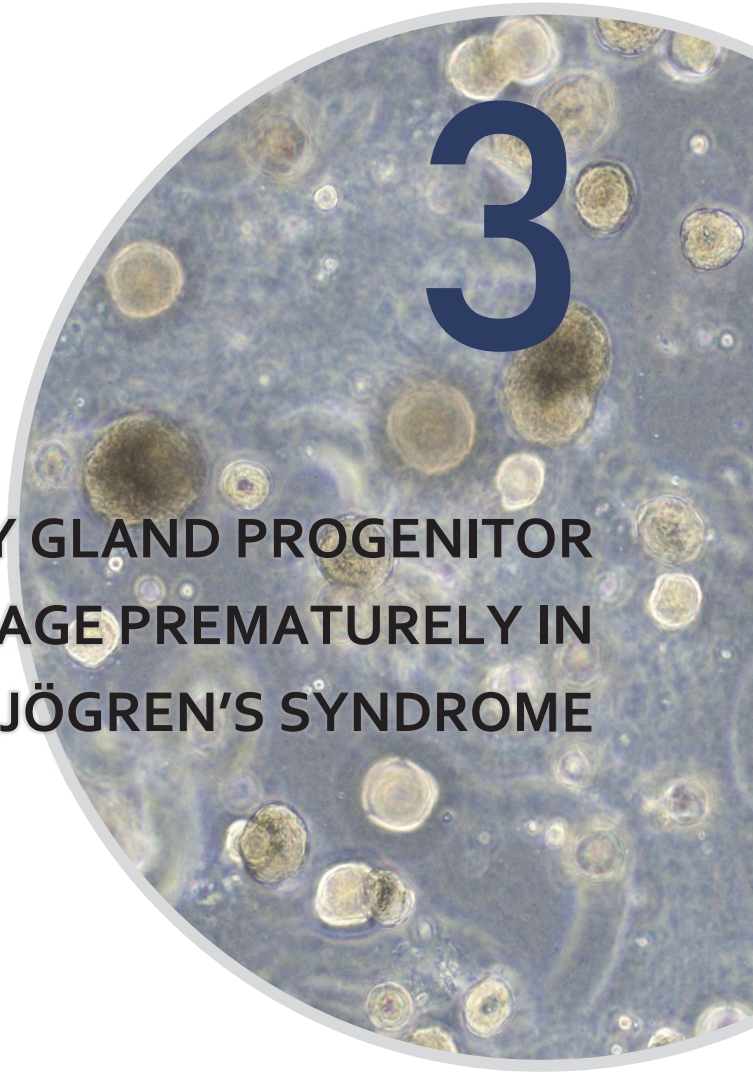

3

SALIVARY GLAND PROGENITOR CELLS AGE PREMATURELY IN PRIMARY SJÖGREN'S SYNDROME

*Sarah Pringle, **Xiaoyan Wang**, Gwenny M.P.J. Verstappen, Janneke H. Terpstra, Clarence K. Zhang, Aiqing He, Vishal Patel, Rhiannon E. Jones, Duncan M. Baird, Fred K. L. Spijkervet, Arjan Vissink, Hendrika Bootsma, Robert P. Coppes, Frans G.M. Kroese.*

Arthritis Rheumatol. 2019, 71: 133-142.

ABSTRACT

Objective A major characteristic of the autoimmune disease primary Sjögren's syndrome (pSS) is salivary gland (SG) hypofunction. The inability of resident SG progenitor cells (SGPCs) to maintain homeostasis and saliva production has never been explained and limits our comprehension of mechanisms underlying pSS. The present study was undertaken to investigate the role of salivary gland progenitor cells in hyposalivation in pSS.

Methods SGPCs were isolated from parotid biopsy samples from controls and patients classified as having pSS or incomplete pSS, according to the American College of Rheumatology/European League Against Rheumatism criteria. Self-renewal and differentiation assays were used to determine SGPC regenerative potential, RNA was extracted for sequencing analysis, single telomere length analysis was conducted to determine telomere length, and frozen tissue samples were used for immunohistochemical analysis.

Results SGPCs isolated from pSS parotid gland biopsy samples were regeneratively inferior to healthy control specimens. We demonstrated that SGPCs from samples from patients with pSS are not only lower in number and less able to differentiate, but are likely to be senescent, as revealed by telomere length analysis, RNA sequencing, and immunostaining. We further found that SGPCs exposed to pSS-associated proinflammatory cytokines we induced to proliferate, express senescence-associated genes, and subsequently differentiate into intercalated duct cells. We also localized $p16^{+}$ senescent cells to the intercalated ducts in pSS SG tissue, suggesting a block in SGPC differentiation into acinar cells.

Conclusion This study represents the first characterization of SGPCs in pSS, and also the first demonstration of a linkage between an autoimmune disease and a parenchymal premature-aging phenotype. The knowledge garnered in this study indicates that disease-modifying antirheumatic drugs used to treat pSS are not likely to restore saliva production, and should be supplemented with fresh SGPCs to recover saliva production.

1. INTRODUCTION

Between 0.4 and 3.1 million people in the US have been diagnosed as having the autoimmune disease primary Sjögren's syndrome (pSS)[1]. Presenting clinically predominantly in women (9:1 ratio), pSS is a multifaceted syndrome most often associated with production of autoantibodies (SSA/Ro and SSB/La), infiltration

of the salivary glands (SGs) with lymphocytes, and hyposalivation (reduced secretory function of the SGs). Other symptoms may include neurologic involvement, lung symptoms, and chronic fatigue. Lymphocytic infiltration of SGs is characterized and measured clinically by the presence of immune foci, defined as a gathering of >50 lymphocytes in the SGs, associated with the striated ducts[2]. The periductal infiltrates may evolve into ectopic lymphoid tissue harboring germinal centers (sites of memory B cell formation). In addition, the relative number of IgA plasma cells decreases, in parallel with glandular dominance of IgG-producing plasma cells. Mucosa-associated lymphoid tissue lymphomas are also frequently observed in the SG tissue of patients with pSS. These features of salivary gland infiltration reflect the B cell-dominated phenotype of pSS[3]. Given these characteristic lymphocytic infiltrates, the logical conclusion is that lymphocytic infiltration of SGs is the causative factor underlying hyposalivation. However, recent detailed research has clearly demonstrated that the correlation between salivary flow and degree of inflammation is weak[4–10].

In healthy SGs, homeostasis is maintained by proliferation and differentiation of tissue-resident SGPCs. According to one of the prevailing views in the field, these cells for example reside in striated ducts, from where they differentiate first toward intercalated ducts and subsequently to acinar cells[11–15]. Other studies have identified progenitor cell populations within the acinar cell subset, and, alternatively, have suggested that acinar cells themselves are capable of maintaining SG homeostasis through self-replication[16,17]. Regardless of the predominant viewpoints, the apparent lack of ability of SGPCs to maintain SG homeostasis in pSS has never been explained, and likely contributes to hyposalivation development in pSS. In this study, we used protocols for SGPC isolation recently developed by us and others to probe the involvement of SGPCs in pSS[11–13,15,18]. We demonstrate that SGPCs in pSS are likely to be senescent, a phenotype that may be induced by exposure to pSS-associated proinflammatory cytokines.

2. PATIENTS AND METHODS

2.1 Source of salivary gland tissue

For healthy control specimens, biopsy samples of parotid SG tissue were obtained from donors (after informed consent and institutional review board [IRB] approval) who were treated for a squamous cell carcinoma of the oral cavity. In these patients, an elective head and neck dissection procedure was

performed. During this procedure, a parotid SG is exposed and removed. This tissue does not contain malignant cells, as oral squamous cell carcinoma does not disseminate to the parotid SG. To obtain study samples from patients with primary and incomplete pSS, specimens were obtained during the routine diagnostic evaluation for pSS. Patients were classified as having pSS if they fulfilled the 2016 American College of Rheumatology (ACR)/European League Against Rheumatism (EULAR) criteria[19]. Patients classified as having incomplete pSS did not fulfill these criteria and were not taking hyposalivation-inducing medication, but they did demonstrate either objective symptoms of dry mouth or SSA autoantibody presence. IRB approval was obtained, and all patients with pSS and incomplete pSS provided informed consent (METc 2016/010).

2.2 Progenitor cell isolation

Parotid SG biopsy samples harvested from oral squamous cell cancer patients with healthy parotid gland tissue and samples obtained from patients with pSS and incomplete pSS after surgery were processed in Hanks' balanced salt solution (HBSS) containing 1% bovine serum albumin (BSA; Invitrogen). Biopsy samples were digested mechanically using a gentleMACS dissociator (Miltenyi Biotec) or manually with scissors and simultaneously digested in HBSS/1% BSA buffer containing 0.63 mg/ml type II collagenase (Invitrogen) and 0.5 mg/ml hyaluronidase (Sigma-Aldrich), as well as calcium chloride at a final concentration of 6.25 mM, for 30 minutes at 37°C. Forty milligrams of tissue was processed per 1 ml buffer volume; total volume was adjusted according to biopsy sample weight. Digested cells were collected by centrifugation, washed twice in HBSS/1% BSA solution, and passed through 100-µm cell strainers (BD Biosciences).

The resultant cell suspensions were collected again by centrifugation and resuspended in SGPC medium consisting of 40% Dulbecco's modified Eagle's medium/F-12 medium, penicillin/streptomycin antibiotics (Invitrogen), Glutamax (Invitrogen), 50% Wnt-3a-conditioned medium, 10% R-spondin-conditioned medium (derived from the RSPO1 cell line; AMSBIO), 20 ng/ml epidermal growth factor (Sigma-Aldrich), 20 ng/ml fibroblast growth factor 2 (Sigma-Aldrich), N2 (Invitrogen), 10 mg/ml insulin (Sigma-Aldrich), 1 mM dexamethasone (Sigma-Aldrich), 10 µM Rho kinase inhibitor (Abcam), 5 µM transforming growth factor β inhibitor (catalog no. A8301; ToCris Bioscience), and 12.5 ng/ml Noggin (PeproTech). A total of 800,000 primary isolate cells were resuspended in 25 µl of SGPC medium combined with 50 µl of basement membrane Matrigel (BD Biosciences) and deposited in the center of 12-well

tissue culture plates. After the gels were allowed to solidify (20 minutes at 37°C), 1 ml of progenitor cell medium was added per well. After 3-5 days of culture, the formed primary spheres were released from Matrigel by incubation in 1 mg/ml Dispase (Sigma) (1 hour at 37°C). Primary spheres of a minimum size of 50 µM were counted and used to establish primary sphere yield per milligram of biopsy material. To correct primary sphere yield for the site of biopsy, the primary sphere yields for healthy control samples and pSS samples were multiplied by factors of 4.1 and 11.95, respectively. Multiplication factors were derived from the yield of primary spheres isolated from the SGPC-rich area, as described by van Luijk et al[20].

2.3 Cytospot preparation and quantification

A total of 100 µl of cell suspension obtained after SGPC isolation was added into a cytospin funnel, after prewetting of coated microscope slides with 1% BSA/phosphate buffered saline (PBS) solution. After centrifugation at 300 revolutions per minute for 2 minutes, slides were air dried and fixed with 4% paraformaldehyde (PFA) at room temperature for 20 minutes. Hematoxylin and eosin staining was then performed according to standard protocols. The number of acinar and ductal cells was determined by capturing images of 3 areas of the cytospot per sample. The total cell number in each area was determined by counting hematoxylin-stained nuclei. Acinar cells were identified by characteristic triangular morphology and predominant hematoxylin staining. Ductal cells were identified by heavily eosin-stained cytoplasm. The proportion of each cell type was expressed as the percentage of total cells. For $CD45^+$ cell quantification, cytospots were fixed as described above, then permeabilized in 100% ethanol (20 minutes at -20°C), washed in PBS, and then incubated in mouse anti-CD45 antibody (Dako) (1 hour at room temperature), diluted 1:100 in 1% BSA containing 0.05% Tween. Following PBS washing, Alexa Fluor 488-conjugated goat anti-mouse secondary antibody was added onto cytospots at 1:300 dilution in 1% BSA/0.05 PBS containing Tween and incubated at room temperature for 1 hour. Following final PBS washes, nuclei were counterstained with DAPI, and cytospots were visualized using a Leica 6000 Series microscope.

2.4 Flow cytometry and FACS of salivary gland isolate

After isolation, cell suspensions were dispersed to single cells. Cells were immunolabeled with antibodies against the following human proteins, conjugated to fluorophores as indicated: eFluor 660-conjugated epithelial cell adhesion molecule (EpCAM) (1:20; eBioscience), phycoerythrin (PE)-Cy5-

conjugated CD45 (1:50; BioLegend), BUV737-conjugated CD19 (1:50; eBioscience), allophycocyanin (APC)-eF700-conjugated CD3 (1:50; eBioscience), PE-Cy7-conjugated CD56 (1:50; BioLegend), APC-eF780-conjugated CD4 (1:50; eBioscience), PE-Cy7-CD24 (1:20; BioLegend), and fluorescein isothiocyanate-conjugated Ki67 (1:200; ThermoFisher Scientific). For intranuclear staining for Ki67, a Foxp3 Transcription Factor Buffer Set was used, according to the instructions of the manufacturer (eBioscience). Staining for keratin (KRT) 14 and smooth muscle actin (SMA) was performed in 2 steps using rabbit anti-human KRT14 (1:100; Abcam) and mouse anti-human SMA (1:100; Dako) and Alexa Fluor 647-conjugated secondary antibody (1:300). Antibodies were added in a total volume of 100 µl 0.5% BSA/PBS with 2 mM EDTA (staining buffer), containing a maximum of 1 million cells. Staining was performed for 20 minutes on ice. Cells were collected by centrifugation and resuspended in staining buffer for analysis with an LSRII flow cytometer (BD Bioscience).

Living-dead discrimination was performed using 80 ng/ml propidium iodide (ThermoFisher). For FACS sorting of $EpCAM^+$ cells from SG isolate, staining was performed as described above, with the addition of 0.1M magnesium sulfate and 50 µg/ml DNase (both from Sigma) into cell suspension to prevent cell clumping. Collected $CD45^+$ cells were harvested into progenitor cell medium collected by centrifugation and plated into Matrigel as described above. The gating strategy for flow cytometric analysis and FACS is shown in Supplementary Figure S1.

2.5 Self-renewal

Following the release of primary spheres from Matrigel as described above, cells were dispersed to form single-cell suspensions using 0.05% trypsin-EDTA (Invitrogen), enumerated, and concentrations adjusted to 0.4×10^6 cells per ml in SGPC medium. Twenty-five microliters of this cell solution was combined with 50µl volumes of basement membrane Matrigel and deposited in the center of 12-well tissue culture plates. After the Matrigel was solidified for 20 minutes at 37°C, gels were covered in progenitor cell medium as described above. Organoids appeared 2-3 days after seeding of single cells in Matrigel. Ten days after seeding, Matrigel was dissolved by incubation with Dispase enzyme as described above. Organoids >50 µM in diameter were enumerated, cells were processed to a single-cell suspension using 0.05% trypsin-EDTA, and cell numbers were determined. These data were used to generate the organoid formation efficiency and population doublings. Population doublings (pds) were calculated according to the following formula:

$$pds = \frac{\ln 2\,(\text{harvested cells}/\text{seeded cells})}{\ln 2}$$

Encapsulation in Matrigel was repeated to generate the next passage. This cycle was repeated 4 times (4 passages). At the end of each passage, an image of the cells was captured using an Olympus CKX53 microscope and DP2-SAL software.

2.6 Mature organoid formation assay

For mature organoid formation assays, organoid cultures were supplemented with 1 µM isoproterenol. Mature organoid formation was monitored over a 2-week period.

2.7 RNASeq

Total RNA was extracted from progenitor cells using an Absolutely RNA Miniprep Kit (catalog no. 400800), according to the instructions of the manufacturer (Agilent). The integrity of RNA was examined with an Agilent 2100 Bioanalyzer. Subsequent sequencing was performed using a SMART-Seq v4 Ultra Low Input RNA Kit (catalog no. 634890; Clontech) and a Nextera XT DNA Library Prep Kit (catalog no. FC-131-1096; Illumina) according to the instructions of the manufacturers, and prepared DNA libraries were sequenced on a HiSeq 2500 system. Data quality assessment was performed to understand the main source of variability, and differential expression analysis and visualization were performed in R (packages PVCA, EdgeR, and PHeatmap). The MetaCore pathway database was used for pathway enrichment analysis; data can be accessed via the NCBI Sequence Reads Archive (accession no. PRJNA506620).

2.8 Cytokine incubations with SGPCs

Cytokines were purchased as follows: human interleukin-6 (IL-6) (catalog no. 200-06A; PeproTech), human interferon-α (IFNα) (catalog no. 11100-1; R&D Systems), and human tumor necrosis factor (TNF) (catalog no. 300-01A; PeproTech) and reconstituted according to the instructions of the manufacturers. Dilutions for coculture with cytokines were performed in such a manner that the volume of cytokine added to the medium was always 1% of the total medium volume. The medium was refreshed 2 times within the passage (days 3 and 6), in parallel with control cultures.

2.9 Whole mount and tissue immunocytochemistry

Mature organoids were released from Matrigel using Dispase, collected in round-bottomed 96-well plates, and fixed in 2% PFA for 10 minutes. Frozen tissue sections were cut at a thickness of 8 µM and fixed in 2% PFA for 5 minutes. Staining for all samples was performed from this point, using a Tyramide Signal Amplification Kit according to the instructions of the manufacturer (ThermoFisher). After hydrogen peroxide blocking and general blocking, primary antibodies were incubated with organoids, mature organoids, or tissue sections overnight in PBS at 4°C. Dilutions of primary antibodies used for immunostaining were as follows: rabbit anti-human amylase (1:100) (catalog no. A2863; Sigma), rabbit anti-human aquaporin 5, rabbit anti-human EpCAM, mouse anti-human IL-6 receptor (1:100) (clone B-R6; ThermoFisher), mouse anti-human TNF receptor type I (clone H398;ThermoFisher), rabbit anti-human IFNα receptor (1:100) (catalog no. 62693; Abcam), mouse anti-human p16 (1:100) (catalog no. 54210; Abcam), and mouse anti-human SMA (1:100) (catalog no. M0851; Dako). Nuclear counterstaining was performed with Hoechst 33342, at a 1:300 dilution from 10 mg/ml stock solution, for 10 minutes at room temperature. Immunostainings were visualized using a Leica TCS SP8 confocal laser scanning microscope and Leica Application Suite software.

2.10 Telomere analysis

DNA was extracted from human SGPCs using a QIAamp DNA Micro Kit (Qiagen). Single telomere length analysis (STELA) was carried out at the XpYp telomere as described previously by Capper et al[21]. Briefly, 1 µM Telorette 2 linker was added to 10 ng of purified genomic DNA in a final volume of 40 µl per sample. Multiple polymerase chain reactions (PCRs) were performed for each test DNA in 10 µl volumes, incorporating 250 pg of DNA, 0.5 µM telomere-adjacent and Teltail primers, 75 mM Tris HCl (pH 8.8), 20 mM $(NH_4)_2SO_4$, 0.01% Tween 20, 1.5 mM $MgCl_2$, and 0.5 units of a 10:1 mixture of Taq (ABgene) and Pwo polymerase (Roche Molecular Biochemicals). The reactions were processed in a Tetrad2 Thermal Cycler (Bio-Rad). DNA fragments were resolved by 0.5% Tris-acetate-EDTA agarose gel electrophoresis and identified by Southern hybridization with a random-primed a-33P-labeled (PerkinElmer) TTAGGG repeat probe, together with probes specific for the 1 kb (Stratagene) and 2.5 kb (Bio-Rad) molecular weight markers. Hybridized fragments were detected using a Typhoon FLA 9500 Phosphorimager (GE Healthcare). The molecular weights of the DNA fragments were calculated using a Phoretix 1D Quantifier (Nonlinear Dynamics).

2.11 Quantitative PCR (qPCR)

Total RNA was extracted from cultured cells using an RNeasy Microkit, including DNase incubation, according to the instructions of the manufacturer (Qiagen). One microgram of total RNA was reverse transcribed to complementary DNA (cDNA) using 0.5 µg of oligo(dT)$_{15-18}$ primers, 1.0 mM dNTPs, 1× Reaction Buffer, 20 units of RiboLock, and 200 units of RevertAid reverse transcriptase (all from ThermoFisher Scientific) in a total volume of 20 µl per reaction. The cDNA product was diluted 10-fold in water and used at this concentration for qPCR. Qualitative PCR was performed using SsoAdvanced Universal SYBR Green qPCR Master Mix (Bio-Rad), with primers at a final concentration of 500 nM from a 10 µM stock. Diluted cDNA (2.5 µl) was used per reaction, and all reactions were performed in triplicate in a total volume of 10 µl. Primer sequences are shown in Supplementary Table S1. A 2-step qPCR cycle with a Bio-Rad iCycler qPCR machine was used for target amplification, according to the instructions of the manufacturer for SSoAdvanced Universal SYBR Green Master Mix, and CFX Manager was used for analysis.

3.RESULTS

3.1 Salivary gland progenitor cells from pSS patients show reduced regenerative potential

We began by isolating SGPCs from parotid SG biopsy samples from control patients with healthy SGs and patients with pSS fulfilling the ACR/EULAR classification criteria[19]. SGPCs were initially cultured from processed biopsy samples as primary spheres in Wnt-containing medium. Three to 5 days later, spheres were dispersed to single SGPCs and expanded in a “self-renewal assay.” The cell suspension generated by the isolation process from pSS biopsy samples contained significantly fewer epithelial cells than healthy control biopsy samples and significantly more CD45$^+$ leukocytes, based on cell morphology and immunostaining on cytospots (Supplementary Figures S2 and S3A–C). As previously reported for minor SGs, we detected a high proportion of B cells and a predominance of CD4$^+$ T cells within the flow cytometry-defined CD45$^+$ fraction of the biopsy isolate (Supplementary Figure S2D and E)[22]. SGPCs are EpCAM^{high} in nature. The number of both spheres generated per EpCAM^{high} cell and yield of spheres per milligram of biopsy sample was significantly lower (a 10-fold difference) in samples from patients with pSS compared to the healthy samples (Figures 1A and B, and Supplementary Figure S2F). Data are presented as normalized to milligrams of tissue to take into account the larger size of the

healthy SG biopsy samples obtained. Primary sphere yield was not correlated with focus score (lymphocytic infiltration) (Supplementary Figure S2G), supporting the notion that infiltration does not determine SG function. We have previously demonstrated that SGPC yield decreases with age and that more SGPCs are present closest to the facial nerve in the parotid gland[20,23]. Neither donor age nor biopsy site was responsible for the decreased yield of SGPCs from pSS biopsy samples (Supplementary Figures S2H and I).

Progenitor cells are classically defined by their ability to proliferate and differentiate. When SGPCs from pSS biopsies were cultured as organoids to assess their proliferation capacity, we observed a significantly (up to 5 times) lower self-renewal capability compared to healthy samples (Figures 1C-E). FACS selection of $EpCAM^{high}$ cells from pSS biopsies, after removal of infiltrating leukocytes, did not rescue the self-renewal potential of pSS SGPCs (Supplementary Figure S3), indicating that the sole presence of $CD45^{+}$ cells in SGs of patients with pSS is not responsible for the regenerative deficits observed.

Healthy SGPCs could be induced to proliferate and differentiate from organoids into α-amylase-expressing mature organoids (Figures 1F and G). The lack of proliferative capabilities of SGPCs from pSS biopsies was reflected also in their greatly diminished ability to form mature organoids (Figure 1H). These data imply that the relatively few SGPCs present in pSS SGs also harbor defects in differentiation ability.

3.2 Extensive replicative history of salivary gland progenitor cells in pSS

In order to elucidate the early events in SG pathology development in pSS that are not influenced by mass lymphocytic infiltration, we focused on patients have some hallmarks of pSS (outlined in Supplementary Table S2), but do not have a positive lymphocyte focus score in the parotid gland. Also, the patients with incomplete pSS were not taking medication known to cause dry mouth symptoms, they all had recorded symptoms of dry eyes and mouth associated with pSS development, and they did not fulfill the ACR/EULAR criteria. We consider these features indicative of early SG pathology development in pSS. When SGPCs were isolated from the patients with incomplete pSS we observed that the primary sphere yield from a small proportion (2 of 10) of these biopsy samples was markedly greater than the median of the healthy control samples

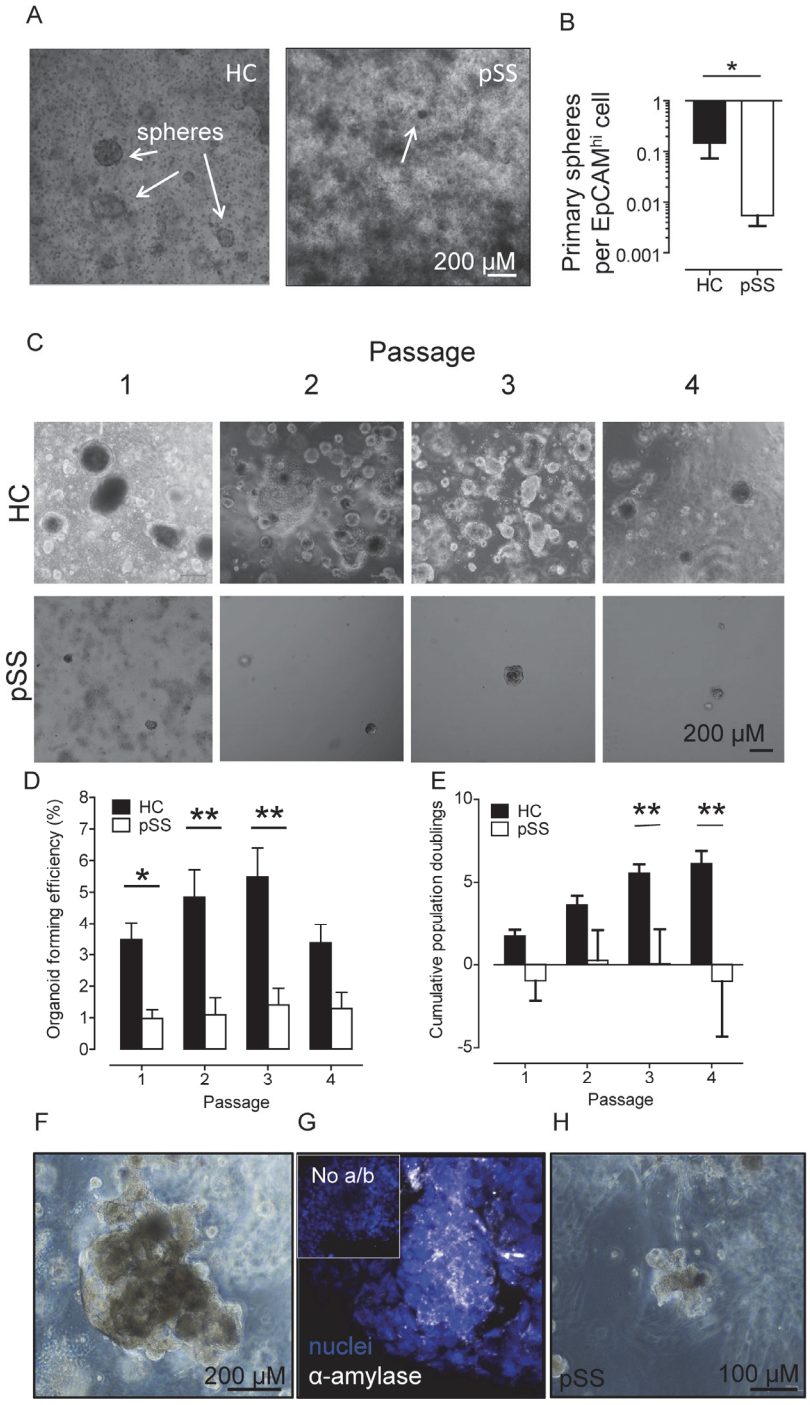
A
HC
spheres
pSS
200 μM
B
*
Primary spheres per EpCAM^hi cell
1
0.1
0.01
0.001
HC
pSS
C
Passage
1
2
3
4
HC
pSS
200 μM
D
Organoid forming efficiency (%)
HC
pSS
*
**
**
Passage
E
Cumulative population doublings
HC
pSS
**
**
Passage
F
200 μM
G
No a/b
nuclei
α-amylase
H
pSS
100 μM

Figure 1 | Salivary gland progenitor cells (SGPCs) from primary Sjögren's syndrom (pSS) patients show reduced regenerative potential.
A) Microscopy of primary spheres isolated from SGPCs from a healthy control (HC) (left) and a patient with pSS (right). Arrows show organoids. **B)** Quantification of primary sphere yield per epithelial cell adhesion molecule ($EpCAM^{high}$) cell in SGPC isolates from biopsy samples from healthy controls (n = 6) and patients with pSS (n = 9). * = $P < 0.05$ by Student's *t*-test. **C)** Microscopy of organoid cultures of SGPCs from a healthy control and a patient with pSS. **D)** Organoid-forming efficiency of SGPCs in cultures of biopsy tissue from healthy controls (n = 27 at passages 1-4) and patients with pSS (n = 12, 16, 9, and 6 at passages 1-4, respectively). * = $P < 0.05$; ** = $P < 0.01$ by two-way analysis of variance (ANOVA) with Bonferroni post hoc testing. **E)** Cumulative population doublings of SGPCs from healthy controls (n = 26 at passages 1-3; n = 24 at passage 4) and patients with pSS (n = 10, 5, 4, and 2 at passages 1-4, respectively). ** = $P < 0.01$ by two-way ANOVA with Bonferroni post hoc testing. **F)** Phase-contrast microscopy of mature organoids formed from SGPCs from a healthy control. **G)** Immunocytochemical staining of acinar cell-associated amylase in a healthy control SG sample-derived mature organoid. Inset shows a healthy control SG sample without anti-amylase antibody (a/b) to demonstrate staining specificity. **H)** Diminished ability to form mature organoids from pSS SGPCs. Values in **B**, **D**, and **E**, are the mean ± SEM.

(Figure 2A). The yield of primary spheres from the remaining biopsy samples was comparable to the biopsy yield from the patients with pSS. Reasoning that the 2 (of 10) patients with the high yield represent an earlier disease stage[24], we theorized that SGPCs receive mitotic stimuli early in pSS. We performed RNA sequencing on organoids cultured from patients with negative focus score to investigate early events in pSS, and we observed a cohort of 101 significantly up-regulated genes in SGPCs from biopsy-negative patients compared to healthy control samples ($p < 0.01$, $\log_{10}$-fold change ≥2) (Figure 2B).

On further examination, we found that 18 of these genes were involved in cell cycle progression (both its promotion and inhibition) and DNA replication (Figure 2C and Figure S4). As shown in Figures 2C and D, the β-galactosidase-like gene GLB1L2 was also significantly up-regulated. Beta galactosidase expression is associated with cellular senescence and aging. Hypothesizing that SGPCs in pSS disease progression become senescent, we examined the telomere lengths of organoids cultured from patients with pSS with positive SG biopsy evaluations (i.e., with lymphocytic infiltration), representing a later phase of pSS in terms of SG pathology. STELA analysis of telomere length revealed short telomeres of <4.5 kb in length in SGPCs from biopsy-positive patients with pSS (Figures 2E and F, and clinical characteristics shown in Table S2). The mean length of the lowest 10% of telomeres in the SGPCs of healthy control samples was significantly

greater (5.58 kb) compared to pSS SGPCs (3.10 kb) (Figure 2G), suggesting that pSS SGPCs have a more extensive replicative history. The mean ages of healthy control sample donors and pSS SGPC donors in whom telomere analysis was performed were 77.3 and 61.5 years, respectively, confirming that telomere difference was not due to the advanced age of SGPC donors with pSS.

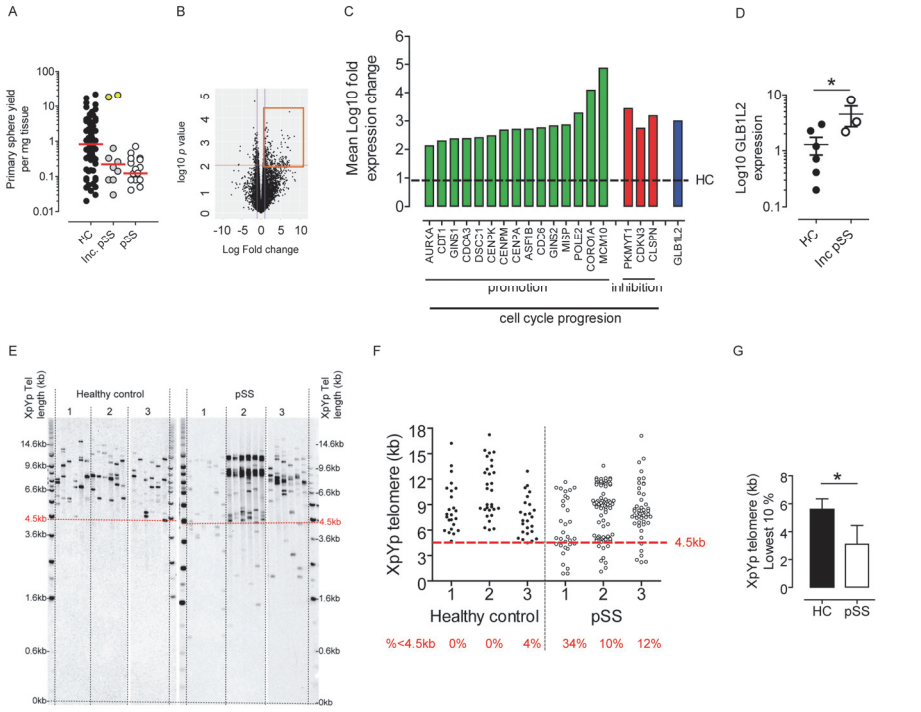

Figure 2 | Salivary gland progenitor cells (SGPCs) from primary Sjögren's syndrome (pSS) patients are more likely to be senescent.

A) Primary sphere yield in SGPCs from healthy controls (HC) (n = 73), patients with incomplete (Inc.) pSS (n = 10), and patients with pSS (n = 18). Symbols represent individual spheres. Yellow circles show SGPCs with unusually high yield. Red lines show the median. **B)** Volcano plot resulting from RNA sequencing analysis comparing SGPC transcriptomes in biopsy samples from healthy controls and pSS patients with negative parotid focuse score. Boxed area denotes genes whose expression is ≥log10 2-fold higher in pSS SGPCs. Red line shows P value cutoff threshold ($P < 0.01$). **C)** Up-regulation of cell cycle progression promotion genes (green) and inhibition genes (red) identified from RNA sequencing, including the β-galactosidase-like gene (GLB1L2) (blue). Broken line represents the mean expression level in healthy controls (n = 6 individual samples from healthy controls; n = 3 samples from patients with pSS. **D)** Raw expression values for GLB1L2. Symbols represent individual samples from healthy controls (n = 6) and patients with pSS (n = 3). Bars show the mean ± SEM. **E)** Single telomere length analysis

of SGPC telomere lengths in biopsy samples from healthy controls and patients with biopsy-proven pSS, showing outlying small (<4.5 kb) telomeres (red dotted line) in pSS SGPCs. **F)** Quantification of telomere lengths in SGPCs from healthy controls and patients with pSS. Red text denotes percentage of telomeres with length <4.5 kb (broken line). Symbols represent individual samples. **G)** Length analysis of lowest 10% of telomeres in SGPCs from healthy controls and patients with biopsy-proven pSS (n = 3 per group). Values are the mean ± SEM. * = P ≤ 0.05 by Student's *t*-test.

3.3 Proinflammatory cytokines induce proliferation and differentiation of healthy salivary gland progenitor cells

pSS is an autoimmune disease associated with the glandular presence of classic proinflammatory cytokines, as exemplified by IFNα, TNF, and IL-6[25,26]. Proinflammatory cytokines within the glandular tissue could provide mitotic signals, driving SGPC exhaustion in pSS and leading to a senescent, aging-like phenotype and ultimately hyposalivation. Considering the low yield of SGPCs from patients with pSS, and in order to model the earliest phases of pSS, we employed healthy control SGPC cultures to investigate this hypothesis. Quantitative PCR and immunostaining of healthy control SGPC organoids at passage 2 demonstrated that healthy control SGPCs express receptors for the proinflammatory cytokines IFNα, TNF, and IL-6 (see Figure S5 and [for primers] Table S1). When healthy control SGPCs from passages 1-4 were incubated with a cocktail of proinflammatory cytokines at concentrations matching those found in the serum of patients with pSS (IFNα 500 pg/ml, TNF 40 pg/ml, and IL-6 30 pg/ml)[27], we observed initially a significant increase in organoid formation efficiency, followed by a decrease to significantly below the levels in control cells (Figures 3A and B). Incubation with single cytokines did not induce significant proliferative effects, even at higher doses (see Figure S6). At passage 1 following cytokine exposure, expression of genes promoting cell cycle progression (CDK4, CDK6, and CDC20), inhibiting cell cycle (E2F1 and CDKN2D), and promoting senescence (p16 and p21) was up-regulated (Figure 3C). Through definition of SGPC subsets using cell surface markers (see Figures S7A-C), we also showed that SGPCs resident in the basal layer of striated ducts (BSD cells) were responsible for the proliferation (marked by Ki67) observed (Supplementary Figure S7D). We also suggest that proinflammatory cytokines induce differentiation of BSD cells into intercalated ducts (ID cells) (Figure S7D and E). Finally, p16 immunostaining was performed on sections of SG tissue in order to determine where senescent cells were located *in situ*; $p16^+$ cells were found mostly in intercalated ducts in incomplete and complete pSS tissue. In contrast,

p16+ cells in healthy SGs were found dispersed through the tissue (Figures 3D-G), illustrating their full differentiation potential.

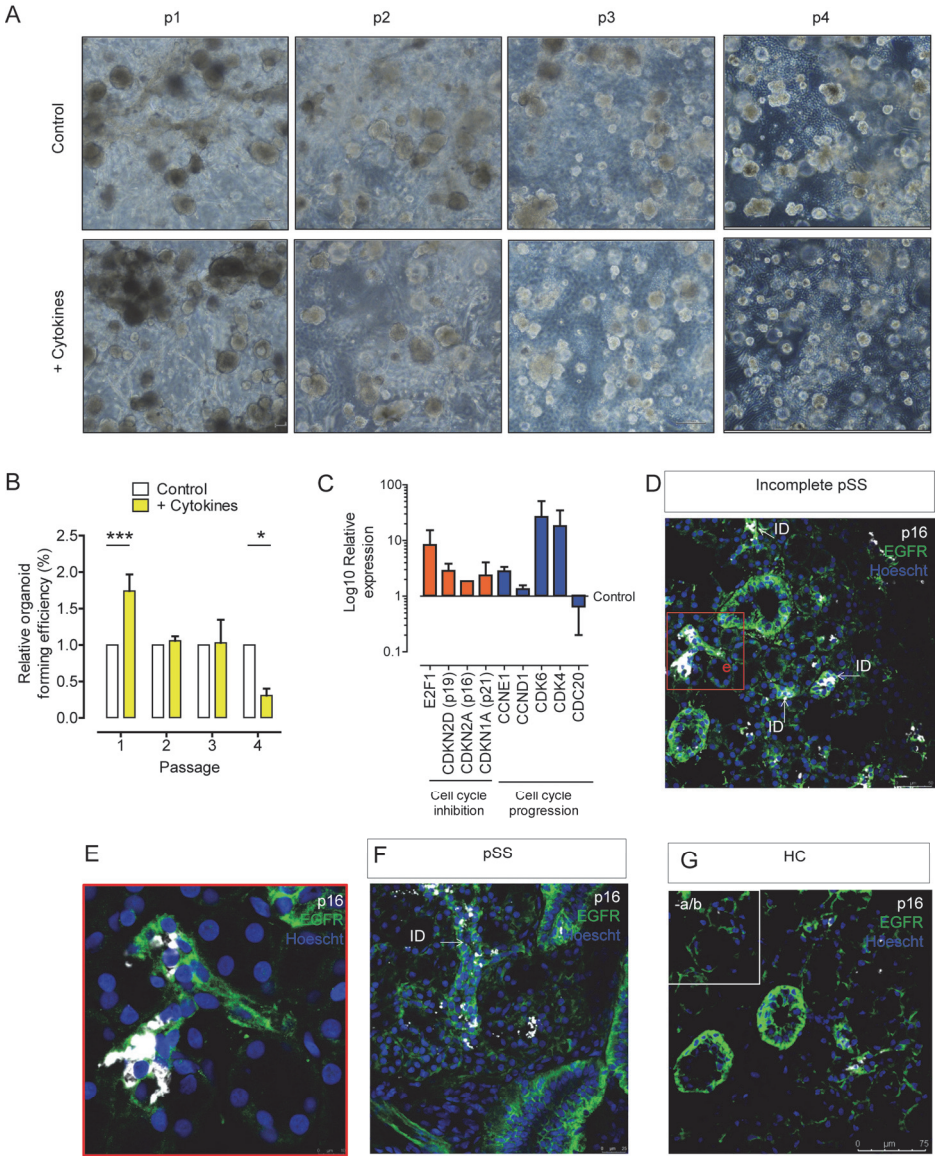

Figure 3 | Parotid salivary gland progenitor cell (SGPC) organoid cultures proliferate upon exposure to a proinflammatory cytokine cocktail and express cell cycle and senescence genes. p16+ senescent cells localize to the intercalated ducts (IDs) in SG tissue from patients with incomplete primary Sjögren's syndrome (pSS) and patients with pSS.

A) Phase-contrast microscopy of SGPCs from a healthy control at passages 1-4, incubated with (+ Cytokines) and without (Control) the proinflammatory cytokine cocktail. **B)** Quantification of organoid formation efficiency of SGPCs exposed to proinflammatory cytokines compared to control cells; (n = ≥7 separate cell sample isolations at each passage). Bars show the mean ± SEM. * = P < 0.05; *** = P < 0.001 by two-way analysis of variance. **C)** Expression of cell cycle-associated genes in SGPCs exposed to proinflammatory cytokines. Cells were harvested at the end of passage 1 for quantitative polymerase chain reaction analysis. Bars show the mean ± SEM (n = 2 separate cell sample isolations). **D)-G)** Immunohistochemical staining for p16 senescence marker in SG tissue from a patient with incomplete pSS (**D**; **D** inset shown in **E**), a patient with pSS (**F**), and a healthy control (HC) (**G**), counterstained with epithelial growth factor receptor (EGFR) to mark all ductal cells. Inset in **G** shows SG tissue from a healthy control without antibody (−a/b) staining, to demonstrate specificity. Ages of tissue donors were 50, 73, and 31 years for the healthy control, patient with incomplete pSS, and patient with pSS, respectively, indicating that the increase in $p16^+$ ID cells could not be attributed to the advanced age of the donor.

4. DISCUSSION

The origins of hyposalivation development in pSS have never been fully elucidated, although many studies have now firmly established that its development cannot be fully explained by the extent of lymphocytic infiltration[4–10]. Using SGPCs as a tool to probe SG dysfunction in pSS, we showed in the present study that parotid gland biopsy samples from patients with pSS contain fewer SGPCs with reduced proliferation, differentiation potential, and shortened telomeres. Shortened telomeres imply that the SGPC pool has an extensive replicative history, the reason for which we propose is 2-fold.

First, the parenchymal epithelium, e.g., the non-progenitor ductal cells and saliva-producing acinar cells in pSS, have been demonstrated to undergo enhanced levels of apoptosis, from sources intrinsic and extrinsic to the cells themselves. Extrinsically, the action of cytokines, cytotoxic T cells, and natural killer cells all promote apoptosis[28]. Additionally, a disorganized extracellular matrix in pSS SGs may account for acinar cell loss by anoikis[29]. Epithelial cells have been shown to intrinsically express defective levels of the antiinflammatory mediator peroxisome proliferator-activated receptor γ, resulting in increased activity of the NFκB and IL-6 pathways, but also rendering them more susceptible to cell death[30–35]. Similarly, levels of the ubiquitin-editing protein A20, a negative regulator of NFκB, were down-regulated in SG epithelial cells from patients with pSS compared to healthy subjects[36]. Therefore, depletion of the parenchymal cell pool via intrinsic and extrinsic mechanisms

together likely stimulates SGPC proliferation and differentiation into acinar cells, in an attempt to maintain the saliva-producing capacity of the SGs.

Second, as we have demonstrated here, proinflammatory cytokines exert a direct effect on proliferation of SGPCs. In other model systems, and most extensively in the well-characterized intestinal progenitor cell niche, proinflammatory cytokines have also been shown to exert a proliferative effect, mediated by modulation of the progenitor cell-associated Wnt, Notch, and Yes-associated protein/transcriptional co-activator with PDZ-binding motif (YAP/TAZ) pathways, suggesting that cross-talk between progenitor cells and the elements of the immune system may underlie many disease manifestations[37–41]. Cytokine production in the case of pSS may be derived from neighboring epithelial cells signaling in a paracrine manner. The production and secretion of proinflammatory cytokines by epithelial cells has been demonstrated in long-term epithelial culture systems and in situ[33,42–45]. Following the release of damage- and pathogen-associated molecular patterns, e.g., molecules such as high mobility group box chromosomal protein 1 and viral antigens, pattern recognition receptors on epithelial cells may be activated, culminating in epithelial cell autonomous NFκB pathway activity, cytokine production, and paracrine signaling to neighboring SGPCs[34,35]. Indeed, the dysregulated NFκB pathway seen in pSS may account for the sustained proinflammatory cytokine production by glandular epithelial cells[34,36].

One prevailing theory regarding progenitor cells dictates that under healthy conditions, SGPCs reside in the striated ducts, proliferate and differentiate into intercalated ducts, and then finally into saliva-producing acinar cells. We have demonstrated the presence of senescent cells in intercalated ducts of pSS SGs. This presence suggests a blockade in the ability of SGPCs to further differentiate into acinar cells, presumably due to having reached their regenerative limit, similar to the poor mature organoid differentiation potential we demonstrated in vitro. Clinically, our data suggest that screening patient SGs or saliva for senescence biomarker expression may indicate the extent of SGPC exhaustion. We further suggest that clinical interventions aimed at preventing hyposalivation development need to occur before the appearance of high levels of senescent markers in SGs or saliva. The present study findings also suggest, critically, that effective interventions to cure established hyposalivation by targeting the inflammatory process are not likely to involve only immune signal blockade, but rather the replenishment of SGPC stocks in conjunction with resolving the inflammation. Plausible strategies include the use of induced pluripotent stem cell technologies in the manufacture of SGPCs.

In conclusion, we have demonstrated for the first time an aging phenotype as a potential causative agent for the lack of SG repair in the autoimmune disease pSS, and link this finding to possible future clinical strategies.

5. ACKNOWLEDGEMENTS

The authors gratefully acknowledge M.J.H. Witjes DMD, MD, PhD and K.P. Schepman DMD, MD, PhD (Department of Oral and Maxillofacial Surgery, University Medical Center Groningen, University of Groningen, Groningen, The Netherlands) for providing the healthy control parotid salivary gland biopsies.

REFERENCES

1. Helmick, C. G. *et al.* Estimates of the prevalence of arthritis and other rheumatic conditions in the United States: Part I. *Arthritis Rheum.* **58**, 15–25 (2008).
2. Segerberg-Konttinen, M., Konttinen, Y. T. & Bergroth, V. Focus score in the diagnosis of Sjögren's syndrome. *Scand. J. Rheumatol. Suppl.* **61**, 47–51 (1986).
3. Kroese, F. G. *et al.* B-cell hyperactivity in primary Sjögren's syndrome. *Expert Rev. Clin. Immunol.* **10**, 483–499 (2014).
4. Jonsson, R. *et al.* Progression of sialadenitis in Sjögren's syndrome. *Br. J. Rheumatol.* **32**, 578–581 (1993).
5. Mignogna, M. D., Fedele, S., Russo, L. Lo, Muzio, L. Lo & Wolff, A. Sjogren's syndrome: the diagnostic potential of early oral manifestations preceding hyposalivation/xerostomia. *J. Oral Pathol. Med.* **34**, 1–6 (2005).
6. Soto-Rojas, A. E. & Kraus, A. The oral side of Sjögren syndrome. Diagnosis and treatment. A review. *Arch. Med. Res.* **33**, 95–106 (2002).
7. Dawson, L. J., Fox, P. C. & Smith, P. M. Sjögrens syndrome—the non-apoptotic model of glandular hypofunction. *Rheumatology* **45**, 792–798 (2006).
8. Theander, E., Andersson, S. I., Manthorpe, R. & Jacobsson, L. T. H. Proposed core set of outcome measures in patients with primary Sjögren's syndrome: 5 year follow up. *J. Rheumatol.* **32**, 1495–1502 (2005).
9. Haldorsen, K., Moen, K., Jacobsen, H., Jonsson, R. & Brun, J. G. Exocrine function in primary Sjogren syndrome: natural course and prognostic factors. *Ann. Rheum. Dis.* **67**, 949–954 (2008).
10. Nikolov, N. P. & Illei, G. G. Pathogenesis of Sjögren's syndrome. *Curr. Opin. Rheumatol.* **21**, 465–470 (2009).
11. Lombaert, I. M. A. *et al.* Rescue of salivary gland function after stem cell transplantation in irradiated glands. *PLoS One* **3**, e2063 (2008).
12. Pringle, S. *et al.* Human salivary gland stem cells functionally restore radiation damaged salivary glands. *Stem Cells* **34**, 640–652 (2016).
13. Pringle, S., Van Os, R. & Coppes, R. P. Concise review: adult salivary gland stem cells and a potential therapy for xerostomia. *Stem Cells* **31**, 613–619 (2013).
14. Xiao, N. *et al.* Neurotrophic factor GDNF promotes survival of salivary stem cells. *J Clin Invest* **124**, 3364–3377 (2014).
15. Maimets, M. *et al.* Long-term in vitro expansion of salivary gland stem cells driven by Wnt signals. *Stem Cell Reports* **6**, 150–162 (2016).
16. Emmerson, E. *et al.* Salivary glands regenerate after radiation injury through SOX2-mediated secretory cell replacement. *EMBO Mol. Med.* **10**, e8051 (2018).
17. Aure, M. H. H., Konieczny, S. F. F. & Ovitt, C. E. E. Salivary gland homeostasis is maintained through acinar cell self-duplication. *Dev. Cell* **33**, 231–237 (2015).
18. Nanduri, L. S. Y. *et al.* Purification and ex vivo expansion of fully functional salivary gland stem cells. *Stem Cell Reports* **3**, 957–964 (2014).
19. Shiboski, C. H. *et al.* 2016 American College of Rheumatology/European League Against Rheumatism classification criteria for primary Sjögren's syndrome. *Ann. Rheum. Dis.* **76**, 9–16 (2017).

20. van Luijk, P. *et al.* Sparing the region of the salivary gland containing stem cells preserves saliva production after radiotherapy for head and neck cancer. *Sci. Transl. Med.* **7**, 305ra147 (2015).
21. Capper, R. *et al.* The nature of telomere fusion and a definition of the critical telomere length in human cells. *Genes Dev.* **21**, 2495–2508 (2007).
22. Mingueneau, M. *et al.* Cytometry by time-of-flight immunophenotyping identifies a blood Sjögren's signature correlating with disease activity and glandular inflammation. *J. Allergy Clin. Immunol.* **137**, 1809-1821.e12 (2016).
23. Maimets, M., Bron, R., de Haan, G., van Os, R. & Coppes, R. P. Similar ex vivo expansion and post-irradiation regenerative potential of juvenile and aged salivary gland stem cells. *Radiother. Oncol.* **116**, 443–448 (2015).
24. Shiboski, C. H. *et al.* Natural history and predictors of progression to Sjögren's syndrome among participants of the Sjögren's international collaborative clinical alliance registry. *Arthritis Care Res.* **70**, 284–294 (2018).
25. Roescher, N., Tak, P. P. & Illei, G. G. Cytokines in Sjögren's syndrome: potential therapeutic targets. *Ann. Rheum. Dis.* **69**, 945–948 (2010).
26. Youinou, P. & Pers, J.-O. Disturbance of cytokine networks in Sjögren's syndrome. *Arthritis Res. Ther.* **13**, 227 (2011).
27. Pollard, R. P. E. *et al.* Predominantly proinflammatory cytokines decrease after B cell depletion therapy in patients with primary Sjögren's syndrome. *Ann. Rheum. Dis.* **72**, 2048–2050 (2013).
28. Manganelli, P. & Fietta, P. Apoptosis and Sjögren syndrome. *Semin. Arthritis Rheum.* **33**, 49–65 (2003).
29. Manoussakis, M. N., Spachidou, M. P. & Maratheftis, C. I. Salivary epithelial cells from Sjogren's syndrome patients are highly sensitive to anoikis induced by TLR-3 ligation. *J. Autoimmun.* **35**, 212–218 (2010).
30. Kyriakidis, N. C. *et al.* Toll-like receptor 3 stimulation promotes Ro52/TRIM21 synthesis and nuclear redistribution in salivary gland epithelial cells, partially via type I interferon pathway. *Clin. Exp. Immunol.* **178**, 548–560 (2014).
31. Manoussakis, M. N. & Moutsopoulos, H. M. Sjögren's syndrome: autoimmune epithelitis. *Best Pract. Res. Clin. Rheumatol.* **14**, 73–95 (2000).
32. Kapsogeorgou, E. K., Abu-Helu, R. F., Moutsopoulos, H. M. & Manoussakis, M. N. Salivary gland epithelial cell exosomes: a source of autoantigenic ribonucleoproteins. *Arthritis Rheum.* **52**, 1517–1521 (2005).
33. Spachidou, M. P. *et al.* Expression of functional Toll-like receptors by salivary gland epithelial cells: increased mRNA expression in cells derived from patients with primary Sjögren's syndrome. *Clin. Exp. Immunol.* **147**, 497–503 (2007).
34. Vakrakou, A. G., Polyzos, A., Kapsogeorgou, E. K., Thanos, D. & Manoussakis, M. N. Impaired anti-inflammatory activity of PPARγ in the salivary epithelia of Sjögren's syndrome patients imposed by intrinsic NF-κB activation. *J. Autoimmun.* **86**, 62–74 (2018).
35. Goules, A. V., Kapsogeorgou, E. K. & Tzioufas, A. G. Insight into pathogenesis of Sjögren's syndrome: Dissection on autoimmune infiltrates and epithelial cells. *Clin. Immunol.* **182**, 30–40 (2017).

36. Sisto, M. *et al.* A failure of TNFAIP3 negative regulation maintains sustained NF-κB activation in Sjögren's syndrome. *Histochem. Cell Biol.* **135**, 615–625 (2011).
37. Nava, P. *et al.* Interferon-γ regulates intestinal epithelial homeostasis through converging β-catenin signaling pathways. *Immunity* **32**, 392–402 (2010).
38. Jeffery, V., Goldson, A. J., Dainty, J. R., Chieppa, M. & Sobolewski, A. IL-6 signaling regulates small intestinal crypt homeostasis. *J. Immunol.* **199**, 304–311 (2017).
39. Karin, M. & Clevers, H. Reparative inflammation takes charge of tissue regeneration. *Nature* **529**, 307–315 (2016).
40. Ando, K. *et al.* Induction of Notch signaling by tumor necrosis factor in rheumatoid synovial fibroblasts. *Oncogene* **22**, 7796–7803 (2003).
41. Cressman, D. E. *et al.* Liver failure and defective hepatocyte regeneration in interleukin-6-deficient mice. *Science* **274**, 1379–1383 (1996).
42. Ittah, M. *et al.* B cell-activating factor of the tumor necrosis factor family (BAFF) is expressed under stimulation by interferon in salivary gland epithelial cells in primary Sjögren's syndrome. *Arthritis Res. Ther.* **8**, R51 (2006).
43. Ittah, M. *et al.* Viruses induce high expression of BAFF by salivary gland epithelial cells through TLR- and type-I IFN-dependent and -independent pathways. *Eur. J. Immunol.* **38**, 1058–1064 (2008).
44. Ogawa, N., Ping, L., Zhenjun, L., Takada, Y. & Sugai, S. Involvement of the interferon-g-induced T cell-attracting chemokines, interferon-g-inducible 10-kd protein (CXCL10) and monokine induced by interferon-g| (CXCL9), in the salivary gland lesions of patients with Sjögren's syndrome. *Arthritis Rheum.* **46**, 2730–2741 (2002).
45. Fox, R. I. *et al.* Cytokine mRNA expression in salivary gland biopsies of Sjögren's syndrome. *J. Immunol.* **152**, 5532–5539 (1994).

SUPPLEMENTARY TABLES AND FIGURES

Supplementary Table S1 | Primers.

Gene name	Gene symbol	Forward primer	Reverse primer
Tyrosine-3-monoxygenase	YWHAZ	ttcttgatccccaatgcttc	agttaagggccagacccagt
Interferon-α receptor 1	IFNAR1	cttcaggccaggagttcaag	ctgggtagggaaaggaaagc
Tumor necrosis factor-α receptor -1	TNFRSR1A	ggagtgagaggccatagctg	gttcctttgtggcacttggt
Interluekin-6 receptor	IL6R	ggcaggttgtggaatctgtt	aagaccaccaactccacctg
Cyclin-dependent kinase 4	CDK4	gaaactctgaagccgaccag	aggcagagattcgcttgtgt
Cyclin-dependent kinase 6	CDK6	agagacaggagtggccttga	tgaaagcaagcaaacaggtg
Cyclin inhibitor 1A	CDKN1A	atgaaattcacccccttttcc	ccctaggctgtgctcacttc
Cyclin inhibitor 2A	CDKN2A	atatgccttcccccactacc	cccctgagcttccctagttc
Cyclin inhibitor 2D	CDKN2D	cttccaatccatctggcagt	ctcttgctggagagggtgac
E2F1	E2F1	atgttttcctgtgccctgag	atctgtggtgagggatgagg
Cyclin D1	CCND1	gaggaagaggaggaggagga	gagatggaaggggaaagag
Cyclin E1	CCNE1	agcggtaagaagcagagcag	tttgatgccatccacagaaa
Cell Division Cycle 20	CDC20	gtctgaccatgagcccagat	ctgaggtgatgggttggtct

Supplementary Table S2 | Clinical characteristics of patients donating biopsies for data presented in Figure 2.

Patient	Dry mo-uth complaints	Dry eye complaints	Parotid gland histopathology	SSA autoanti-body titre	Unstimula-ted whole saliva drop	Ocular dryness	Echo score	ACR-EULAR score	Classifi-cation	Figure used in
1	1	1	0	1	0	0	0	3	Inc. pSS	2a
2	1	1	0	1	0	0	0	3	Inc. pSS	2a
3	1	1	0	0	1	1	ND	1	Inc. pSS	2a
4	1	1	0	0	1	1	ND	2	Inc. pSS	2a
5	1	1	0	0	1	1	0	2	Inc. pSS	2a
6	1	1	0	0	1	1	0	1	Inc. pSS	2a
7	1	1	0	0	1	1	ND	2	Inc. pSS	2a
8	1	1	0	0	1	1	0	2	Inc. pSS	2a
9	1	1	0	0	1	1	0	2	Inc. pSS	2a
10	1	1	0	1	1	1	ND	5	pSS	2a, b-d
11	1	1	0	1	1	1	0	4	pSS	2b-d
12	1	1	0	1	1	1	1	5	pSS	2b-d
13	1	1	1	1	1	1	0	8	pSS	2e-g
14	1	1	1	0	1	1	ND	5	pSS	2e-g
15	1	1	1	1	1	0	1	7	pSS	2e-g

Dry mouth complaints were defined as need to drink water during the night, Histopathology was considered positive if the focus score (identified as number of mononuclear infiltrates containing≥50 lymphocytes/4 mm^2 of glandular tissue) was ≥1. Serum levels of anti-SSA/Ro and anti-SSB/La antibodies were assessed with ELISA tests. Unstimulated whole saliva (UWS) drop was evaluated by measuring the saliva production in 15 min. UWS≤1.5 mL/15 min was considered abnormal. Ocular dryness assessed using both an abnormal ocular staining score (OSS) of ≥5 or a Schirmer's test result of ≤ 5 mm/5 minutes. Ultrasound was scored using the Hocevar *et al* scoring system, as validated in Mossel *et al*, Annals Rheumatic Diseases, 2017. Classification was performed according to ACR-EULAR criteria and clinical characteristics presented. With a score of ≥ 4, the patient is classified as pSS. A score of ≤ 3 results in classification of incomplete pSS. Histopathology and autoantibody titre are weighted with 3 points each. ND = no data. '0' and '1' in table represent a negative or positive result for the relevant test, respectively. Inc. pSS = incomplete pSS.

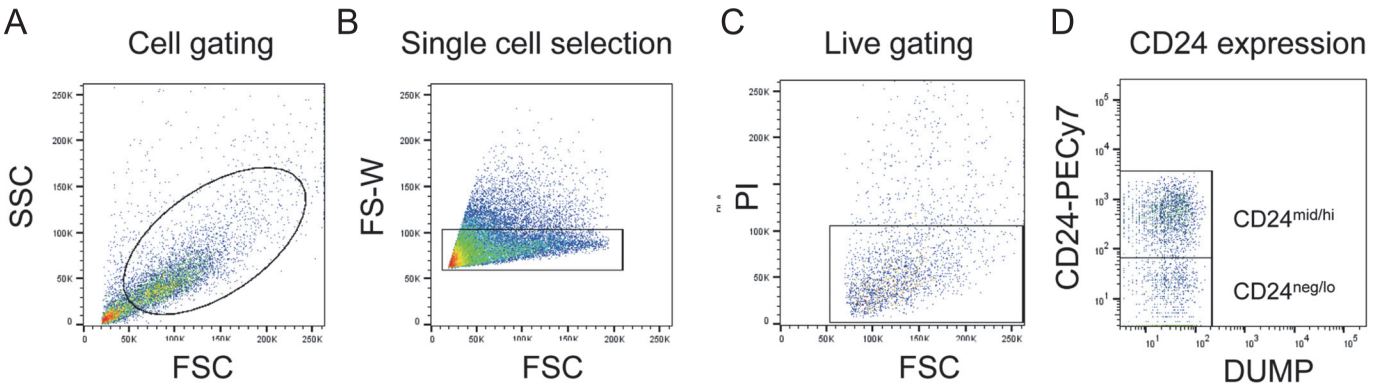

Supplementary Figure S1 | Gating strategy used for flow cytometry.
Cells were **A**) first gated on forward and side scatter axes, **B**) doublets were discriminated, **C**) live dead discrimination performed with Fixable Viability Dye or Propidium Iodide **D)** gated for analysis of CD24 or Ki67 expression.

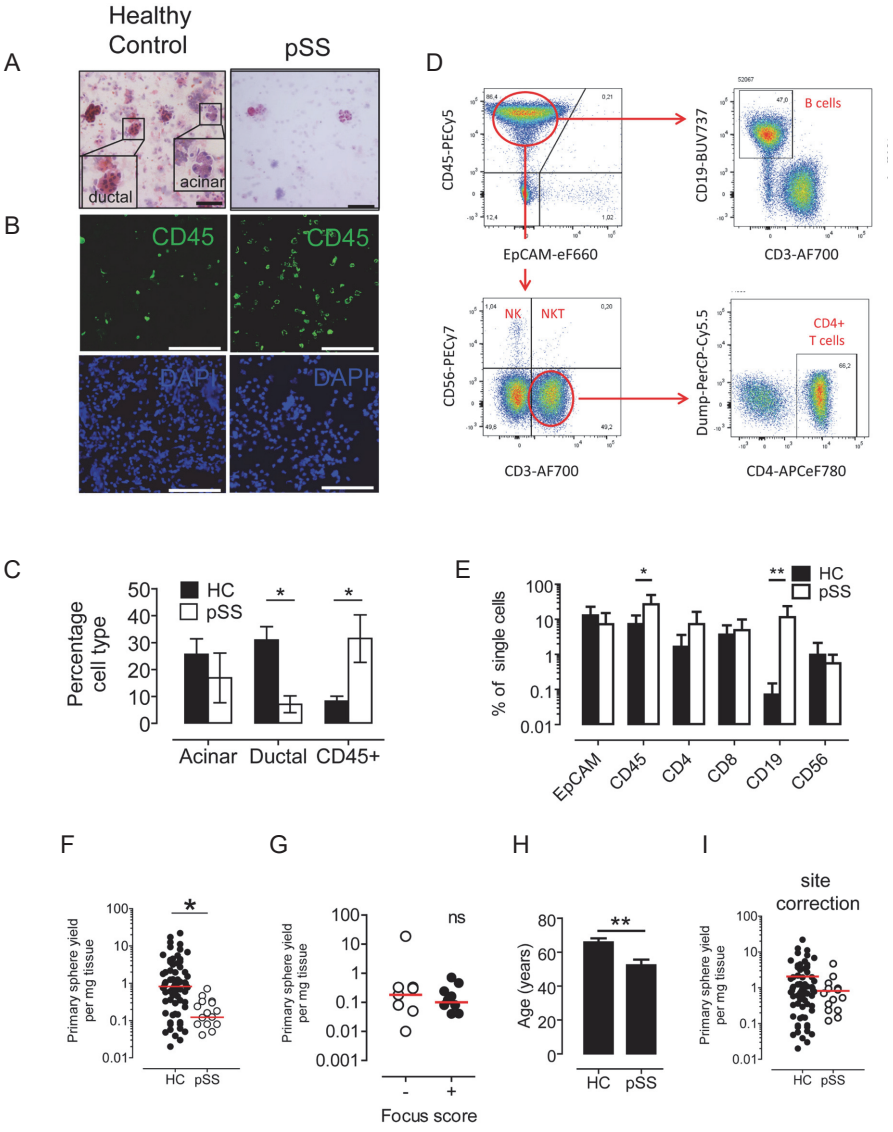

Supplementary Figure S2 | SGPC isolate from pSS biopsies contains less ductal cells, more CD45⁺ leukocytes and generates less organoids per EpCAM⁺ cell.
A) Haematoxylin and eosin staining of cytospots made from final cell solution after SGPC isolation protocol. Ductal and acinar cells were identified on basis of morphology, and indicated in inset boxes in healthy control panel. **B**) Proportion of CD45⁺ leukocytes was determined by immune labeling of cytospots. Top row of B shows single CD45 staining, bottom row all cells, identified by DAPI nuclear staining. **C**) Quantification of proportion of acinar, ductal and CD45⁺ cells. *n* = 10 for healthy controls, 5 for ACR-EULAR criteria

diagnosed primary Sjogren's syndrome samples. Error bars are S.E.M. Scale bars in all images are 100 μM. **D**) Flow cytometry analysis of cell isolate from pSS biopsies, showing high proportion of $CD45^+$ cells, B cells ($CD19^+$) and $CD4^+$ T Cells ($CD3^+CD4^+$). **E**) Summary of proportion of $EpCAM^+$ cells, $CD45^+$ leukocytes, $CD4^+$ T cells, $CD8^+$ T cells, $CD19^+$ B cells, and $CD56^+$ NK cells in isolate generated from processing of pSS and healthy control salivary gland biopsies. *n* = minimum of 6 patients per group per marker. * = $p < 0.05$ ** $p < 0.01$, student's *t*- test. **F**) Primary sphere yield per mg in pSS biopsies compared to HCs. Line represents median value. *n*=29 for HC; 18 for pSS. * = *p* value of 0.0279, student's *t*-test **G**) Primary sphere yield from ACR-EULAR classified pSS biopsies does not differ with positive or negative focus score. *n* = 9 and 10 for focus score negative and positive pSS biopsies respectively. **H**) The ages of HC and pSS patients when their salivary gland biopsies were collected. *n* = 5 and 17 for HC and pSS donors respectively. HC donors are significantly older that pSS donors, suggesting that lower yield from pSS biopsies is not due to advanced age of pSS donors compared to HCs. **I**) Primary sphere from HC and pSS biopsies corrected for optimal site of biopsy harvest. *n* = 72 for HC group and 17 for pSS group.

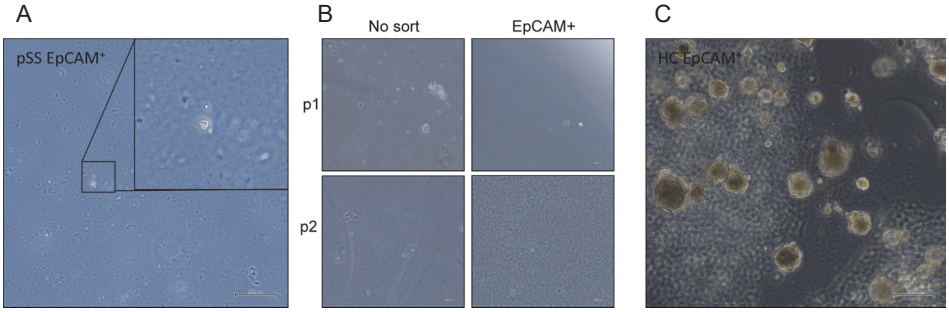

Supplementary Figure S3 | Removal of $CD45^+$ infiltrate from pSS isolate does not rescue proliferative potential of pSS-SGPCs.
A) $EpCAM^+$ cells isolated from a pSS biopsy and cultured. Presence of phase-bright (alive) cells can be observed, which do not appear to proliferate. **B**) Attempts at passaging $EpCAM^+$ cells sorted from pSS biopsies did not rescue growth. **C**) $EpCAM^+$ cells sorted and passaged from healthy control (HC) biopsies grow as organoids following FACS sorting. Lack of growth of pSS derived $EpCAM^+$ cells is therefore not due to damage during sorting.

A

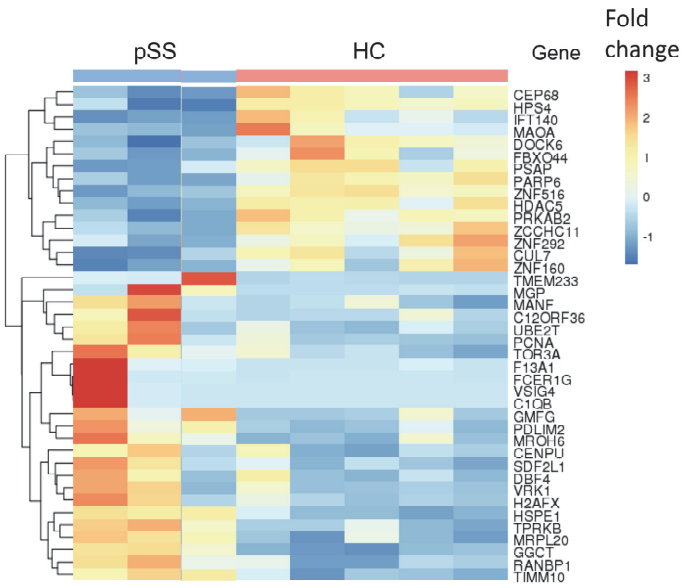

B

#	Maps	-log(pValue)	pValue	FDR	Ratio
1	Transcription_Epigenetic regulation of gene expression		1.695e-5	6.662e-3	6/57
2	Cell cycle_Sister chromatid cohesion		5.237e-5	1.029e-2	4/22
3	Colorectal cancer (general schema)		1.849e-4	1.879e-2	4/30
4	NETosis in SLE		2.107e-4	1.879e-2	4/31
5	Cell cycle_Start of DNA replication in early S phase		2.391e-4	1.879e-2	4/32
6	Transport_Macropinocytosis regulation by growth factors		3.422e-4	1.945e-2	5/63
7	Immune response_Antigen presentation by MHC class I: cross-presentation		3.779e-4	1.945e-2	6/99
8	Ovarian cancer (main signaling cascades)		3.960e-4	1.945e-2	5/65
9	Transcription_Assembly of RNA Polymerase II preinitiation complex on TATA-less promoters		6.417e-4	2.802e-2	3/18
10	Development_Role of HGF in hematopoietic stem cell mobilization		1.024e-3	3.793e-2	3/21
11	Development_PIP3 signaling in cardiac myocytes		1.062e-3	3.793e-2	4/47
12	Role of selected IFN-gamma-inducible genes in cancer pathophysiology		1.578e-3	5.167e-2	5/88
13	Cell cycle_Transition and termination of DNA replication		2.160e-3	6.530e-2	3/27
14	DNA damage_ATM / ATR regulation of G2 / M checkpoint		2.402e-3	6.744e-2	3/29
15	DNA damage_Role of Brca1 and Brca2 in DNA repair		2.936e-3	7.692e-2	3/30
16	DNA damage_ATM/ATR regulation of G1/S checkpoint		3.537e-3	8.688e-2	3/32
17	Development_HGF-dependent inhibition of TGF-beta-induced EMT		4.208e-3	9.729e-2	3/34

Supplementary Figure S4 | Further RNASeq profiling of SGPCs reveals upregulation of pathways involved in cell cycle regulation and DNA damage.
A) Heatmap of 40 differentially expressed genes ($p < 0.001$) between pSS and HCs. Colour coding of differential expression fold changes is given in the legend. **B**) Metacore pathway analysis of RNASeq data identified potential pathways enriched in SGPCs from pSS SG biopsies. ($p < 0.005$, based on 222 genes).

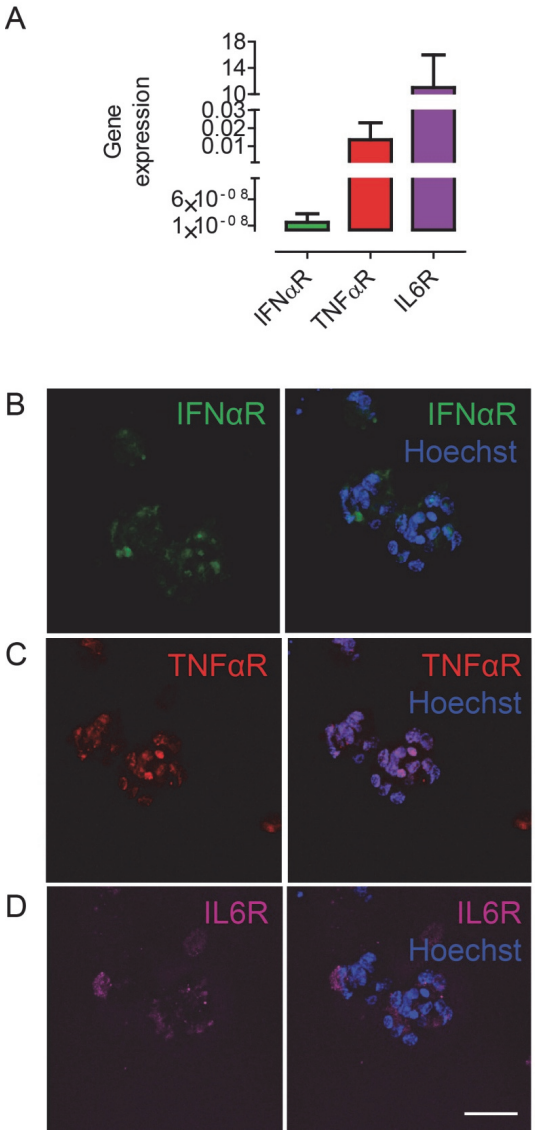

Supplementary Figure S5 | SGPCs express IFNα, TNFα and IL6 receptors.
A) Expression of IFNα, TNFα and IL6 receptors as determined by qPCR. *n* = 3 separate patient biopsies. Inflamed human tonsil cDNA was used as a positive control, and all expression expressed in relation to tonsil. **B-D**) Whole mount microscopy of healthy SGPCs showing expression of the IFNα, TNFα and IL6 receptors. Receptor colour as indicated in panels. First panel shows single colour channel used for the relevant receptor, second a merged image with Hoechst. Scale bar = 50 μM.

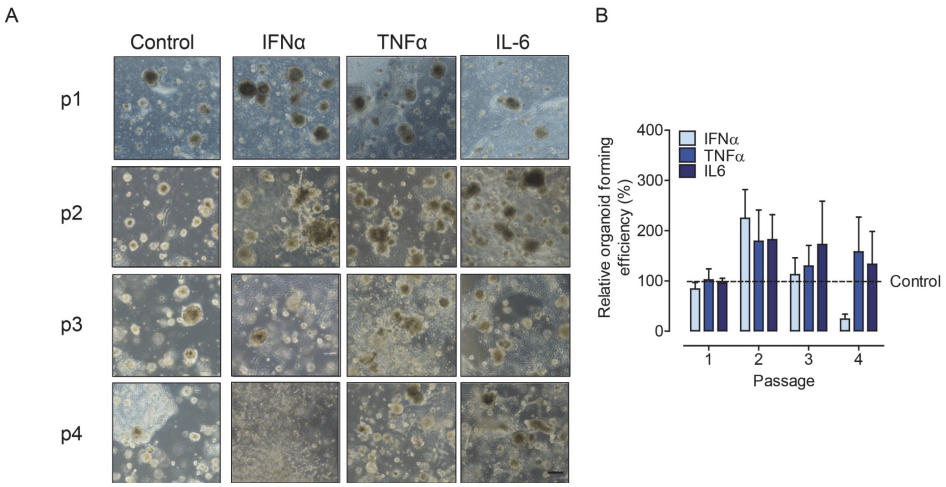

Supplementary Figure S6 | Incubation of SGPCs with single proinflammatory cytokines IFNα, TNFα and IL6 does not induce significant proliferation.

A) Representative phase contrast microscopy of healthy control SGPCs organoids exposed to IFNα (1 ng/mL), IFNɣ (0.1 pg/mL), TNFα (1 ng/mL) and IL-6 (10 ng/mL) at passages 1-4. Scale bar represents 200 µM and applies to all images. **B**) Quantification of proliferation index of cytokine co-cultures. A minimum of 4 distinct biopsies were incubated with each cytokine, and proliferation index determined at every passage. Bar height represents mean, error bars represent SEM. Two Way-ANOVA testing was performed, * = $p < 0.05$.

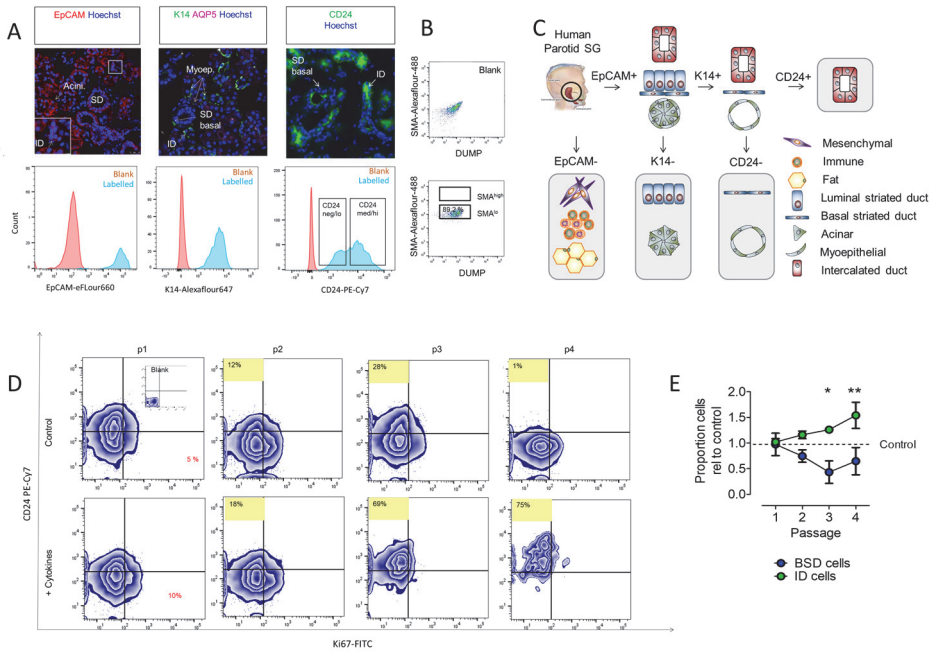

Supplementary Figure S7 | SGPC cultures contain a mixture of basal striated duct cells and intercalated duct cells. Proinflammatory cytokine exposure induces proliferation of the basal striated duct cells, and their differentiation into intercalated duct cells.
A) Immunostaining of healthy parotid tissue and flow cytometric analysis of SGPCs culture for EpCAM, KRT14 and CD24, respectively. KRT14 labelling is counterstained with AQP5 for definition of tissue. ID = intercalated duct. SD = striated duct. **B**) Flow cytometric analysis of a SGPC culture for expression of smooth muscle actin (SMA), a marker protein of myoepithelial cells. SGPC culture were mid-positive to SMA, as opposed to established high positivity of myoepithelial cells. **C**) Schematic showing logical basis for statement that SGPC organoid cultures contains mixture of SGPC from the striated and intercalated ducts, which can be defined ultimately by CD24 expression. Stock human head image adapted from the Blausen library. **D**) Flow cytometric analysis of Ki67 and CD24 expression in SGPCs exposed to proinflammatory cytokines, compared to untreated controls. An initial increase in proliferation ($Ki67^+$) of basal striated duct (BSD) cells was observed. Red text highlights increased proportion of $Ki67^+$ ID cells at p1 following cytokine exposure. Yellow boxed text highlights increasing proportion of $CD24^+$ ID cells following cytokine exposure. Inset box shows blank staining control. **E**) Quantification of proportion of BSD cells and ID cells following SGPC treatment with cytokines. n = ≥ 4 separate patients isolations per group and time point. * $p > 0.05$, ** $p > 0.01$, Two Way ANOVA.